MATERIALS CHEMISTRY
FRONTIERS

RESEARCH ARTICLE

View Article Online
View Journal | View Issue

Cite this: *Mater. Chem. Front.*, 2021, **5**, 4596

Crystalline porphyrin-based graphdiyne for electrochemical hydrogen and oxygen evolution reactions†

Qingyan Pan,‡ Xinsheng Chen,‡ Hui Liu, Weijin Gan, Naixiu Ding* and Yingjie Zhao *

Received 20th February 2021,
Accepted 29th March 2021

DOI: 10.1039/d1qm00285f

rsc.li/frontiers-materials

Two-dimensional graphdiyne (GDY) materials bearing functional photoelectric units have gained much attention due to their unique 2D structure and the sp hybridized carbon. Herein, we prepared a crystalline porphyrin-based graphdiyne through Glaser–Hay coupling reactions. The accurate structure information was acquired through the SAED analysis and simulation. By simply treating with a Co^{2+} solution, the Co-loaded porphyrin-graphdiyne (**CoPor-GDY**) could be easily obtained and can serve as a bifunctional electrocatalyst for the hydrogen evolution reaction (HER) and the oxygen evolution reaction (OER) in alkaline solution. Numerous electrocatalytic sites from Co-porphyrin moieties cooperate with the rapid transport of the butadiyne groups. In addition, the extended 2D porous structure of **CoPor-GDY** could provide effective transporting channels for the diffusion of small molecules and finally lead to efficient catalytic performance. **CoPor-GDY** exhibited an overpotential of 308 mV at 10 mA cm^{-2} and a Tafel slope of 68 mV dec^{-1} for the HER and an overpotential of 400 mV at 10 mA cm^{-2} and a Tafel slope of 129 mV dec^{-1} for the OER. This work explored a new route for the design of a non-noble metal-coordinated GDY analogue electrocatalyst for new energy devices.

Introduction

Exploring efficient, inexpensive, and environmentally friendly electrocatalysts for the hydrogen/oxygen evolution reaction (HER/OER) has attracted great attention.[1,2] In the past few decades, numerous electrocatalysts have been designed and synthesized and are mainly categorized into noble-metal-based[3–8] and carbon-based materials.[9–16] For the noble-metal-based electrocatalysts, they normally exhibit extremely low overpotential and a small Tafel slope, which brings good electrocatalytic performance. However, the disadvantages such as the high manufacturing cost and them suffering from corrosion susceptibility to acidic electrolytes are always obstacles to large-scale commercialization.[2,3] On the other hand, metal-free carbon-based materials have gained much attention and have been considered as a new promising class of electrocatalysts for water splitting due to their tunable chemical/electronic structures and high tolerance to acidic/alkaline conditions.[2,11] But, most of them cannot function both in the HER and OER, and some of them even face the obstacle of low catalytic efficiency (high overpotential and a high Tafel slope).[3,11] Therefore, developing new HER/OER electrocatalysts featuring low-cost, stability and high performance is a long-standing goal.[11]

Graphdiyne (GDY) is a new carbon allotrope composed of sp and sp^2 hybridized carbon atoms.[17] As a novel two-dimensional (2D) carbon material, GDY has received widespread attention since the pioneering work reported by Li and co-workers in 2010.[17] Due to the rich sp hybridized carbon, extended 2D π-conjugated plane, and uneven surface charge distribution, GDY has demonstrated intensive application potential in various research studies of traditional and new fields, such as energy storage and conservation,[18–22] catalysis,[23–28] electronic devices[29–34] and other applications.[35] Many studies have revealed that GDY or GDY/metal composite materials as electrocatalysts have exhibited excellent catalytic activity and good stability for water splitting or the nitrogen reduction reaction.[36,37] For example, Ni/Fe anchored GDY,[38] Fe/Co layered double-hydroxide (LDH) nanosheet array composited GDY,[39] and MoS_2 composited GDY.[40] In addition, GDY analogs containing different functional moieties as metal-free electrocatalysts have also been reported.[41–43] Their interesting characteristics, properties, and applications have also been intensively investigated.

Engineering Research Center of High Performance Polymer and Molding Technology, Ministry of Education, College of Polymer Science and Engineering, Qingdao University of Science and Technology, Qingdao 266042, China. E-mail: nxding1717@163.com, yz@qust.edu.cn

† Electronic supplementary information (ESI) available: Synthesis procedures, electrochemical measurments, ^{1}H-NMR spectra, MS, HR-TEM, *etc.* See DOI: 10.1039/d1qm00285f

‡ These authors contributed equally to this work.

The chemical modified and functionalized-GDYs have been considered as enhanced electrocatalysts in the oxygen reduction reaction (ORR).[44,45] For example, triazine-based GDY has been applied as a high-performance supercapacitor electrode and shows a good performance in catalysing the ORR.[46] Trifluorobenzene-based GDY used as a metal-free catalyst displayed excellent performance for overall water splitting.[47] Based on the above discussion, these well-known functional units together with the unique diacetylene linkages provide us an ideal approach for the preparation of high-performance electrocatalysts and studying the exact HER/OER mechanisms.

Porphyrins possess a delocalized 18-π electron (for the shortest cyclic path) system with unique photophysical and redox properties, and metal coordination characteristics.[10,48] Porphyrins have been widely used as key molecular building blocks in material chemistry due to their symmetry, substitution, metalation, and complexation, which provide many levers to control their organization.[10] Most importantly, the porphyrin structure can stabilize almost all high-valent and low-valent metal ions,[49,50] which is generally believed as a key intermediate for oxidizing and reducing catalytic cycles.[51] However, as a small molecule, porphyrin possesses poor stability, mass transfer issues and low density of catalytic active sites which seriously hinder the applications as electrocatalysts.[52] Therefore, porphyrin-based GDY (**Por-GDY**) with π-conjugated and extended 2D networks may combine the advantages of both GDY and porphyrin and overcome the instability and less catalytic active sites of the small molecule porphyrin compounds. The diacetylene linkages could enhance the electron transfer efficiency, which will result in enhanced electrocatalytic activity.

Herein, we report the targeted synthesis of 2D **Por-GDY** *via* Glaser coupling reaction with the assistance of Cu foil as a template. The Co-loaded **Por-GDY** (**CoPor-GDY**) could be achieved by simply treating with $CoCl_2$ solution in DMF, which was then used as a heterogeneous electrocatalyst for meeting the requirements of the HER and OER. The experimental results revealed that the as-prepared **CoPor-GDY** exhibited relatively low overpotentials for both the HER and OER in alkaline solution. This work provides a simple method for the rational design of bifunctional/multifunctional electrocatalysts to achieve different catalytic effects.

Results and discussion

The 2D **Por-GDY** was prepared by an alkyne–alkyne homocoupling reaction through a bottom-up strategy (Scheme 1). The whole procedure is similar to the synthesis approach of GDY. For details, see the ESI.† Briefly, the freshly cleaned Cu foils were directly added into the pyridine solution, and the solution was heated to 80 °C. Then the pyridine solution of the monomer was added into the solution slowly. The system was kept at this temperature for 3 days. And then a uniform dense dark film was observed on the surface of the Cu foils. The low concentration of monomer was employed here to control the reaction rate. The mechanism of the formation of the **Por-GDY** films was proposed (elaborated in the ESI†). In the beginning, the concentration of Cu(II) ions and monomers is very diluted, so the heterogeneous nucleation and polymerization occurred preferentially on the surface of the Cu foils. The nucleation can minimize the interfacial energy barrier and subsequently lead to the growth of **Por-GDY** on the surface of the Cu foils. **CoPor-GDY** was subsequently obtained by the solvothermal method from $CoCl_2$ and **Por-GDY** in DMF. The as-synthesized **Por-GDY** and **CoPor-GDY** films are stable and insoluble in common organic solvents.

The XPS results reveal the chemical composition and chemical state of the elements existing within **Por-GDY** and **CoPor-GDY**. As shown in Fig. 1a, **Por-GDY** is mainly composed of carbon and nitrogen with an intensity ratio of 7.2 : 1, which is close to the predicted ratio of 7 : 1. The atomic content of Co in **CoPor-GDY** was determined to be 5.45% from the XPS spectrum which is larger than the theoretical value (3.03%).[53,54] The reasons could be the adsorption of the cavities in **Por-GDY** and the complexation with the alkyne groups.[24,39] Besides, the presence of Co 2p in the spectrum of **CoPor-GDY** suggests that the Co species have successfully embedded within the porphyrin rings (Fig. 1b).[55] Fig. S3 (ESI†) presents a high-resolution asymmetric C 1s XPS spectrum of **Por-GDY** and **CoPor-GDY**, which results from the overlapping of the signals of several carbon species with close binding energies. The experimental curve is fitted with four subpeaks at 284.5, 285.3, 286.9, and 288.6 eV assigned to the orbital of C=C (sp^2), C≡C (sp), C=O and C–O, respectively. And the area ratio of the sp/sp^2 carbon is 2/5, which agrees with the theoretical values. The small amounts of oxygen originate from the adsorption from air, which can also be observed from other carbon materials. Furthermore, Fig. 1c shows a high-resolution N 1s XPS spectrum of **CoPor-GDY**, which can be deconvoluted into two subpeaks at 398.8 and 400.1 eV, corresponding to the pyrrolic N and Co–N. Compared with that of **Por-GDY** (Fig. S4, ESI†), N 1s of **CoPor-GDY** gives peaks located at 398.8 eV (pyrrolic N) and 399.9 eV (pyrrolic N–H), and the area ratio of them is almost 1 : 1, which agrees with the molecular structure of porphyrin.

The Raman spectra were performed to reveal the chemical structure information of **Por-GDY** and **CoPor-GDY** (Fig. 1d). The peaks at 1005, 1070, 1235, 1335, 1457 and 1540 cm^{-1} confirm the vibration of the porphyrin group in these two materials.[56] The peak at 2180 cm^{-1} can be assigned to the vibration of the conjugated diyne links (–C≡C–C≡C–). Interestingly, there is a significant decrease at this peak in **CoPor-GDY** (red curve in Fig. 1d), which indicated a possible interaction of the Co and acetylene groups.[57] Moreover, the FTIR spectra further verified the structure of the as-prepared **Por-GDY** (Fig. S5, ESI†). In the UV–vis absorption spectra, there is a significant red shift at the maximum absorption wavelength of **Por-GDY** and **CoPor-GDY**, compared with that of compound 1, which indicated the extension of π-conjugation in **Por-GDY** (Fig. S6, ESI†).

Scanning electron microscopy (SEM) and transmission electron microscopy (TEM) were used to confirm the morphology of the as-obtained materials. Fig. 2a–d revealed the compact film morphologies of the as-obtained **Por-GDY** and **CoPor-GDY**.

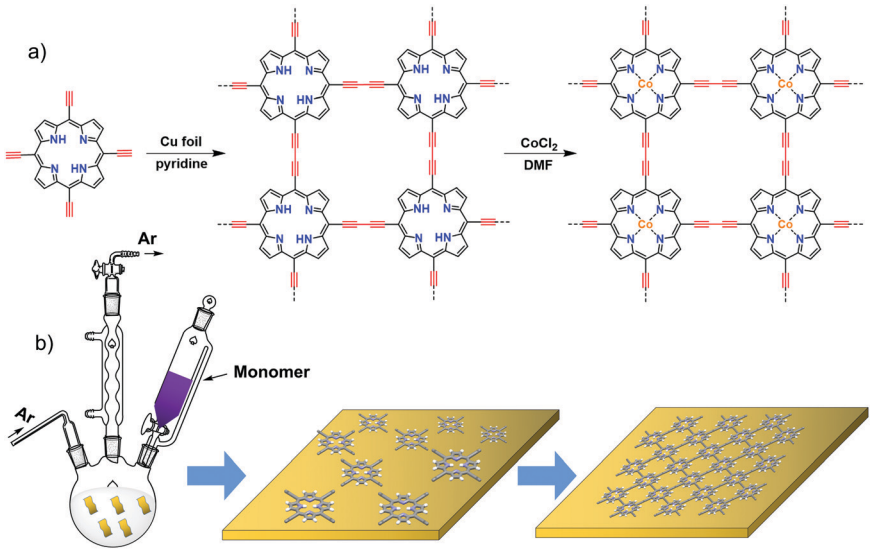

Scheme 1 (a) Synthetic route of **CoPor-GDY**; (b) illustration of the growth process for **Por-GDY**.

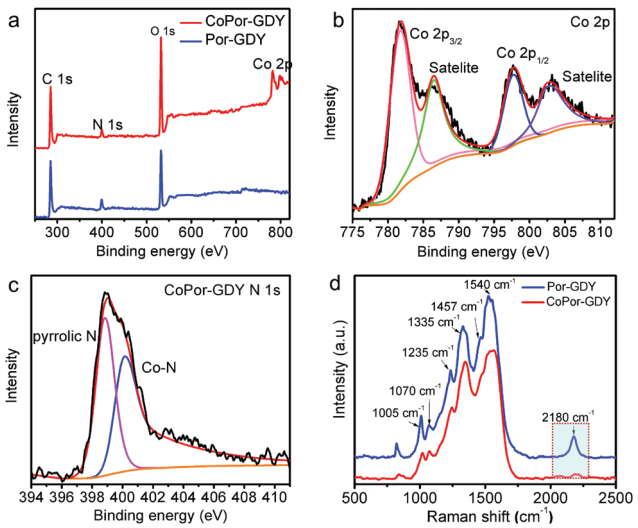

Fig. 1 XPS spectra: (a) full survey of **Por-GDY** and **Co/Por-GDY**. (b) Co 2p (Co $2p_{3/2}$, Co $2p_{1/2}$ and Satellite) for **CoPor-GDY**. (c) N 1s (pyrrolic N and Co–N) for **CoPor-GDY**. (d) The Raman spectra of **CoPor-GDY** and **CoPor-GDY**.

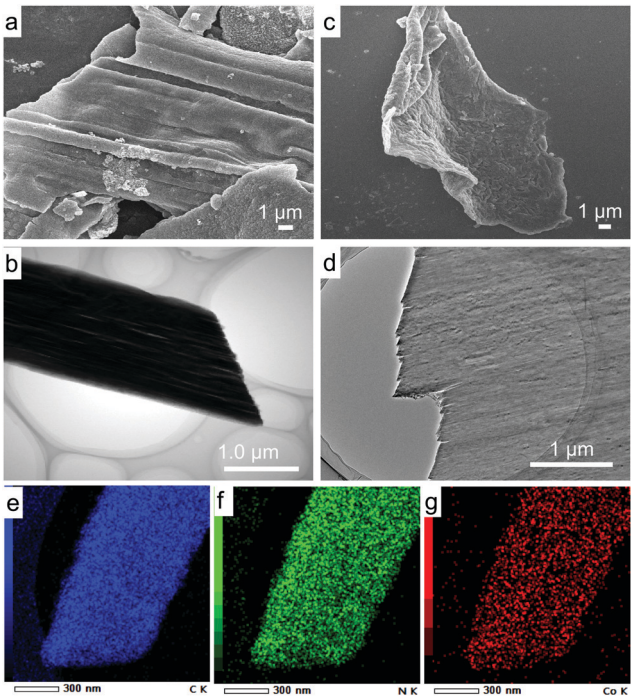

Fig. 2 Morphologies and elemental composition of the as-synthesized materials. (a) SEM image and (b) TEM image for **Por-GDY**. (c) SEM image and (d) TEM image for **CoPor-GDY**. (eg) The EDS elemental mapping of **CoPor-GDY**.

Furthermore, Fig. 2e–g displayed the EDS elemental mapping results; carbon, nitrogen and Co are uniformly distributed in the nanosheets of **CoPor-GDY**. As shown in high-resolution TEM (Fig. S7, ESI†), there are no metal particles observed on the **Por-GDY** plane, which indicates the high dispersion of Co. The deprotonated porphyrins with the proper size can easily coordinate many transition metal ions to form a four-coordinated structure (metal–N_4). Additionally, the sp hybridization of –C≡C– in **Por-GDY** enables the arbitrary angle rotation of π/π^* perpendicular to the axis, making it possible to point toward metal atoms and, thereby, chelate a single metal atom.[38,58] These two characteristics make the Co ultra-uniform and highly dispersed in the 2D plane of **Por-GDY**.

In order to acquire the accurate structure information of the obtained **Por-GDY**, we then performed a selected area electron diffraction (SAED) experiment from the TEM measurements. As shown in Fig. 3, the SAED patterns of both **Por-GDY** and **CoPor-GDY** reveal square lattices with the same *d*-spacing of 0.94 nm (Fig. 3a and b). The SAED pattern of **CoPor-GDY** is similar to that of **Por-GDY**, which indicated the same structures of them. To determine the 2D structure corresponding to the

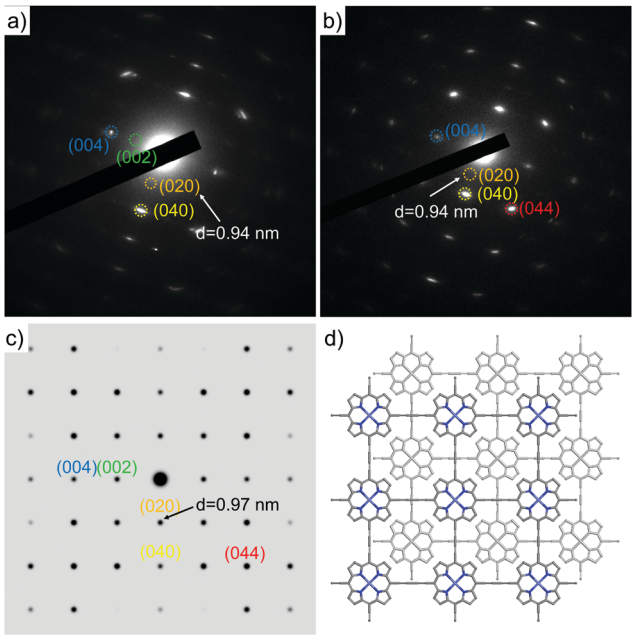

Fig. 3 The SAED patterns for (a) **Por-GDY** and (b) **CoPor-GDY**. (c) Simulated diffraction pattern. (d) The top view of the AB stacked structure.

quadrilateral SAED patterns, we built a model with AB stacking mode which has the same square periodicity as **Por-GDY** (Fig. 3d). The *d*-spacing calculated from the simulated diffraction pattern is 0.97 nm (Fig. 3c), which is highly consistent with the experimental value. It is evident that the structure of **Por-GDY** matches with the AB stacking mode. The thermal treatment in the DMF solution with $CoCl_2$ doesn't influence the stacking structure. Thus, both **Por-GDY** and **CoPor-GDY** were confirmed with AB manner stacking (Fig. 3d and Table S1, ESI†).

The electrocatalytic properties of **Por-GDY** and **CoPor-GDY** for the HER and OER were then determined using a typical three-electrode electrochemical system. **Por-GDY** and **CoPor-GDY** were loaded on carbon cloth (**CC**) under the same conditions, which were used directly as working electrodes. The electrocatalytic performance of **CC** was also investigated as a control experiment. The polarization curves were recorded by linear sweep voltammetry (LSV) tests with a scan rate of 5 mV s^{-1} in 1.0 M KOH solution to get an overpotential at the current density of 10 mA cm^{-2}, which is commonly used to evaluate the electrocatalytic performance of catalysts. As shown in Fig. 4a, **CoPor-GDY** exhibited an onset potential of 115 mV and a low overpotential of 308 mV *versus* the reversible hydrogen electrode (RHE), which is significantly lower than those of the pure **CC** (724 mV) and **Por-GDY** (570 mV). The Tafel plot is used to evaluate the kinetics of the electrocatalytic reaction, and the smaller Tafel slope signifies the faster reaction kinetics. The results suggest that the Tafel slope of **CoPor-GDY** is about 68 mV dec^{-1}, which is much smaller than that of **Por-GDY** (234 mV dec^{-1}) and the pure **CC** (288 mV dec^{-1}) (Fig. 4b). More interestingly, the overpotential of **CoPor-GDY** is comparable to or even lower than those of the reported state-of-the-art porous polymer-based catalysts (Fig. 4c). At a constant applied potential of 320 mV, **CoPor-GDY** shows approximately 96% retention of current density even after 7 h (Fig. S8a, ESI†), suggesting the good long-term stability of **CoPor-GDY**. Furthermore, we also investigated the OER performance of **CoPor-GDY**, as shown in Fig. 4d–f and Fig. S8b (ESI†). **CoPor-GDY** shows an onset potential of 196 mV at the current density of 1.0 mA cm^{-2} and an overpotential of 400 mV at the current density of 10 mA cm^{-2}. **CoPor-GDY** displays a Tafel slope of 129 mV dec^{-1}, which is much smaller than those of **Por-GDY** (475 mV dec^{-1}) and the pure **CC** (248 mV dec^{-1}), as shown in Fig. 4e. The stability of the OER performance was determined in 1.0 M KOH; there is only a very slight decrease observed in the current density (Fig. S8b, ESI†). In comparison with some reported non-noble metal-based catalysts, metal-free porous material catalysts, and even their composites, **CoPor-GDY** exhibited a preferable lower overpotential in the OER (Fig. 4f). All these results indicate that the introduction of Co species in **Por-GDY** has enhanced its performance for the HER and OER in alkaline solution. Meanwhile, the electrocatalytic performances of **CoPor-GDY** in acidic and neutral solutions are not as good as in alkaline solution conditions (Fig. S9, ESI†).

The catalytic kinetics of the as-prepared catalysts were assessed by electrochemical impedance spectroscopy (EIS) analysis (Fig. S10a, ESI†). The typical Nyquist plots of **CoPor-GDY** and **Por-GDY** at an open-circuit voltage are shown in Fig. 4g. The recorded impedance data were fitted by using a circuit model (Fig. S10b, ESI†). **CoPor-GDY** has the smallest solution resistance (R_s = 2.0 Ω) and charge-transfer resistance (R_{ct} = 375.9 Ω) compared to those of **Por-GDY** (R_s = 2.3 Ω and R_{ct} = 1266 Ω) and **CC** (R_s = 2.6 Ω and R_{ct} = 1690 Ω), indicating the faster charge-transfer efficiency which helps to improve the catalytic performance. To further investigate the differences of the electrocatalytic activity of **CoPor-GDY**, **Por-GDY** and pure **CC**, the electrochemically active surface area (ECSA) values of these three samples were measured *via* electrochemical double-layer capacitors (C_{dl}) by cyclic voltammetry experiments, with different scan rates of 20, 40, 60, 80 and 100 mV s^{-1}. The current density at 0.17 V *vs.* RHE is plotted as a function of the scan rate (Fig. 4h). It can be seen that the C_{dl} value of **CoPor-GDY** (5.0 mF cm^{-2}) is higher than those of **Por-GDY** (3.2 mF cm^{-2}) and pure **CC** (3.9 mF cm^{-2}). The results indicate that **CoPor-GDY** possesses more active sites for the redox process, which results in enhanced electrocatalytic HER and OER performances. All these performances are closely related to the structures of the catalysts. Here, both the exposed axial unoccupied positions of the Co atom and the square planar Co–N_4 moieties in **CoPor-GDY** are ideal electrocatalytic active centers.[51,59] As authenticated in many previous reports, the subtle metal atoms–C(sp) bonding in **CoPor-GDY** could be understood as strong (sp)-d orbital charge overlaps, which were also considered to be helpful for conductivity and catalytic activity.[38,58,60] Meanwhile, the acetylenic linkages of the **Por-GDY** structure will enhance the electron transfer efficiency between the Co-porphyrin units, which is undoubtedly able to further improve the electrocatalytic activity of **CoPor-GDY**. In addition, the extended 2D porous plane is conducive to the escape of small molecular products and charge transfer in the

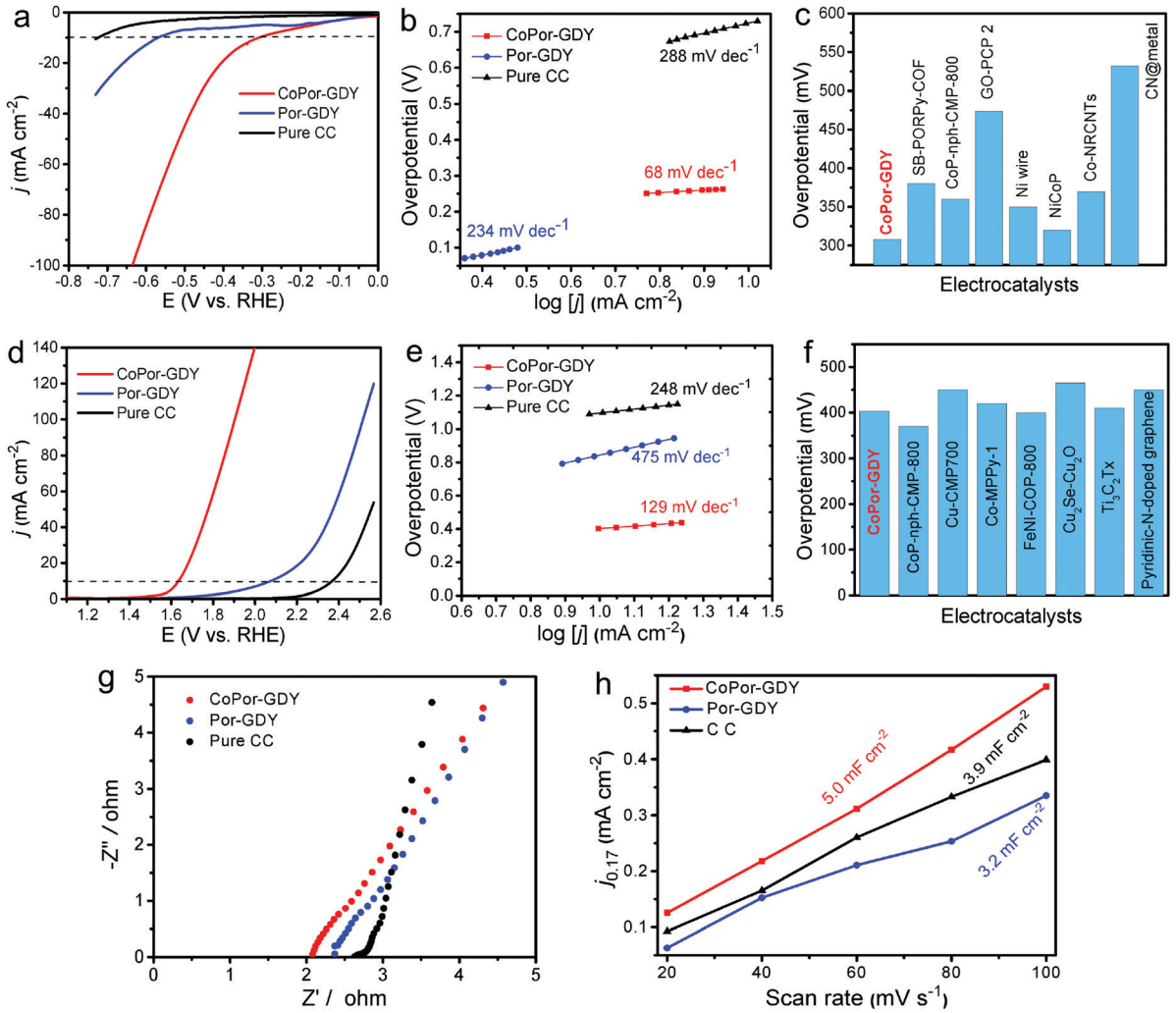

Fig. 4 The electrocatalytic performances of **CoPor-GDY**, **Por-GDY** and pure **CC**. (a) HER LSV curves; (b) the corresponding Tafel plots; (c) comparison of the HER performances of **CoPor-GDY** with the reported catalysts; (d–f) OER LSV curves, the corresponding Tafel plots and comparison of the OER performances of **CoPor-GDY** with the reported catalysts, respectively; (g) Nyquist plots of the catalysts; (h) capacitive current of the samples as a function of scan rate.

plane during the catalytic process. In addition, the 3D structure of **CC** can increase the specific surface area of the **CoPor-GDY** based electrodes, suggesting more catalytic active centers than on the plane substrates. We propose that the porous structure and conductivity of the materials as well as the Co–N_4 moieties as active centers in **CoPor-GDY** are beneficial to enhance the mass transfer of reactants and products, which is very important for high catalytic activity. In addition, the wettability measurements indicate that **CoPor-GDY** has the best hydrophilicity which ensures the good contact between the aqueous solution and the catalyst surface. This facilitates the catalytic reaction for H_2 or O_2 regeneration (Fig. S11, ESI†).

Conclusions

In summary, we designed and synthesized a novel porphyrin-unit-based graphdiyne analog with Co-coordinated loaded porphyrin-graphdiyne, which possesses a highly conjugated and porous structure in a 2D plane. The unique distribution of pores and metal coordination ability of porphyrins provided numerous Co-species active centers endowing **CoPor-GDY** with enhanced electrocatalytic performance in the HER and OER. The commercial **CC** also provided a robust 3D porous conductive substrate and can further improve the electrocatalytic activity because of the fast and facile molecules/ions/gases transportation. **CoPor-GDY** loaded on **CC** used as a working electrode for the electrocatalytic reaction in alkaline solution exhibited an overpotential of 308 mV and a Tafel slope of 68 mV dec^{-1} for the HER and an overpotential of 400 mV and a Tafel slope of 129 mV dec^{-1} for the OER. The metal loaded **Por-GDY** is comparable to or even better than lots of porous polymer-based electrocatalysts. The ternary system formed by transition-metal, GDY analogue and carbon cloth explores a promising way to construct high-performance electrocatalysts in the HER and OER.

Conflicts of interest

There are no conflicts to declare.

Acknowledgements

The work was supported by the National Natural Science Foundation of Shandong Province (No. ZR2020ZD38).

Notes and references

1 R. Borup, J. Meyers, B. Pivovar, Y. S. Kim, R. Mukundan, N. Garland, D. Myers, M. Wilson, F. Garzon, D. Wood, P. Zelenay, K. More, K. Stroh, T. Zawodzinski, J. Boncella, J. E. McGrath, M. Inaba, K. Miyatake, M. Hori, K. Ota, Z. Ogumi, S. Miyata, A. Nishikata, Z. Siroma, Y. Uchimoto, K. Yasuda, K. Kimijima and N. Iwashita, Scientific aspects of polymer electrolyte fuel cell durability and degradation, *Chem. Rev.*, 2007, **107**, 3904–3951.

2 Z. W. Seh, J. Kibsgaard, C. F. Dickens, I. Chorkendorff, J. K. Norskov and T. F. Jaramillo, Combining theory and experiment in electrocatalysis: Insights into materials design, *Science*, 2017, **355**, 4998.

3 B. E. Conway and B. V. Tilak, Interfacial processes involving electrocatalytic evolution and oxidation of H_2, and the role of chemisorbed H, *Electrochim. Acta*, 2002, **47**, 3571–3594.

4 M. E. Lyons and S. Floquet, Mechanism of oxygen reactions at porous oxide electrodes. Part 2-Oxygen evolution at RuO_2, IrO_2 and $Ir_xRu_{1-x}O_2$ electrodes in aqueous acid and alkaline solution, *Phys. Chem. Chem. Phys.*, 2011, **13**, 5314–5335.

5 N. Danilovic, R. Subbaraman, K. C. Chang, S. H. Chang, Y. Kang, J. Snyder, A. P. Paulikas, D. Strmcnik, Y. T. Kim, D. Myers, V. R. Stamenkovic and N. M. Markovic, Using Surface Segregation to design stable Ru-Ir oxides for the oxygen evolution reaction in acidic environments, *Angew. Chem., Int. Ed.*, 2014, **53**, 14016–14021.

6 T. Audichon, E. Mayousse, S. Morisset, C. Morais, C. Comminges, T. W. Napporn and K. B. Kokoh, Electroactivity of RuO_2—IrO_2 mixed nanocatalysts toward the oxygen evolution reaction in a water electrolyzer supplied by a solar profile, *Int. J. Hydrogen Energy*, 2014, **39**, 16785–16796.

7 J. X. Wang, Y. Zhang, C. B. Capuano and K. E. Ayers, Ultralow charge-transfer resistance with ultralow Pt loading for hydrogen evolution and oxidation using Ru@Pt core-shell nanocatalysts, *Sci. Rep.*, 2015, **5**, 12220.

8 Z. Ma, Y. Zhang, S. Liu, W. Xu, L. Wu, Y.-C. Hsieh, P. Liu, Y. Zhu, K. Sasaki, J. N. Renner, K. E. Ayers, R. R. Adzic and J. X. Wang, Reaction mechanism for oxygen evolution on RuO_2, IrO_2, and RuO_2@IrO_2 core-shell nanocatalysts, *J. Electroanal. Chem.*, 2018, **819**, 296–305.

9 Y. Zheng, Y. Jiao, L. H. Li, T. Xing, Y. Chen, M. Jaroniec and S. Z. Qiao, Toward design of synergistically active carbon-based catalysts for electrocatalytic hydrogen evolution, *ACS Nano*, 2014, **8**, 5290–5296.

10 K. Wang, D. Qi, Y. Li, T. Wang, H. Liu and J. Jiang, Tetrapyrrole macrocycle based conjugated two-dimensional mesoporous polymers and covalent organic frameworks: From synthesis to material applications, *Coord. Chem. Rev.*, 2019, **378**, 188–206.

11 L. Dai, Metal-free carbon electrocatalysts: recent advances and challenges ahead, *Adv. Mater.*, 2019, **31**, 1900973.

12 X. Liu and L. Dai, Carbon-based metal-free catalysts, *Nat. Rev. Mater.*, 2016, **1**, 16064.

13 T. N. Ye, L. B. Lv, X. H. Li, M. Xu and J. S. Chen, Strongly veined carbon nanoleaves as a highly efficient metal-free electrocatalyst, *Angew. Chem., Int. Ed.*, 2014, **53**, 6905–6909.

14 Y. Jia, L. Zhang, A. Du, G. Gao, J. Chen, X. Yan, C. L. Brown and X. Yao, Defect graphene as a trifunctional catalyst for electrochemical reactions, *Adv. Mater.*, 2016, **28**, 9532–9538.

15 K. Gong, F. Du, Z. Xia, M. Durstock and L. Da, Nitrogen-doped carbon nanotube arrays with high electrocatalytic activity for oxygen reduction, *Science*, 2009, **323**, 760–764.

16 H. Jiang, J. Gu, X. Zheng, M. Liu, X. Qiu, L. Wang, W. Li, Z. Chen, X. Ji and J. Li, Defect-rich and ultrathin N doped carbon nanosheets as advanced trifunctional metal-free electrocatalysts for the ORR, OER and HER, *Energy Environ. Sci.*, 2019, **12**, 322–333.

17 G. Li, Y. Li, H. Liu, Y. Guo, Y. Li and D. Zhu, Architecture of graphdiyne nanoscale films, *Chem. Commun.*, 2010, **46**, 3256–3258.

18 N. Wang, X. Li, Z. Tu, F. Zhao, J. He, Z. Guan, C. Huang, Y. Yi and Y. Li, Synthesis and electronic structure of boron-graphdiyne with an sp-hybridized carbon skeleton and its application in sodium storage, *Angew. Chem., Int. Ed.*, 2018, **57**, 3968–3973.

19 N. Wang, J. He, Z. Tu, Z. Yang, F. Zhao, X. Li, C. Huang, K. Wang, T. Jiu, Y. Yi and Y. Li, Synthesis of chlorine-substituted graphdiyne and applications for lithium-ion storage, *Angew. Chem., Int. Ed.*, 2017, **56**, 10740–10745.

20 H. Shang, Z. Zuo, L. Li, F. Wang, H. Liu, Y. Li and Y. Li, Ultrathin graphdiyne nanosheets grown in situ on copper nanowires and their performance as lithium-ion battery anodes, *Angew. Chem., Int. Ed.*, 2018, **57**, 774–778.

21 F. Wang, Z. Zuo, L. Li, K. Li, F. He, Z. Jiang and Y. Li, Large-area aminated-graphdiyne thin films for direct methanol fuel cells, *Angew. Chem., Int. Ed.*, 2019, **58**, 15010–15015.

22 L. Li, Z. Zuo, F. Wang, J. Gao, A. Cao, F. He and Y. Li, In situ coating graphdiyne for high-energy-density and stable organic cathodes, *Adv. Mater.*, 2020, **32**, 2000140.

23 Y. Fang, Y. Xue, Y. Li, H. Yu, L. Hui, Y. Liu, C. Xing, C. Zhang, D. Zhang, Z. Wang, X. Chen, Y. Gao, B. Huang and Y. Li, Graphdiyne interface engineering: highly active and selective ammonia synthesis, *Angew. Chem., Int. Ed.*, 2020, **59**, 13021–13027.

24 Y. Fang, Y. Xue, L. Hui, H. Yu and Y. Li, Graphdiyne@janus magnetite for photocatalysis nitrogen fixation, *Angew. Chem., Int. Ed.*, 2021, **60**, 3170–3174.

25 H. Yu, Y. Xue, L. Hui, C. Zhang, Y. Fang, Y. Liu, X. Chen, D. Zhang, B. Huang and Y. Li, Graphdiyne based metal atomic catalysts for synthesizing ammonia, *Natl. Sci. Rev.*, 2020, DOI: 10.1093/nsr/nwaa213.

26 L. Hui, Y. Xue, H. Yu, Y. Liu, Y. Fang, C. Xing, B. Huang and Y. Li, Highly efficient and selective generation of ammonia and hydrogen on a graphdiyne-based catalyst, *J. Am. Chem. Soc.*, 2019, **141**, 10677–10683.

27 Y. Xue, L. Hui, H. Yu, Y. Liu, Y. Fang, B. Huang, Y. Zhao, Z. Li and Y. Li, Rationally engineered active sites for efficient and durable hydrogen generation, *Nat. Commun.*, 2019, **10**, 2281.
28 Z. Zuo, D. Wang, J. Zhang, F. Lu and Y. Li, Synthesis and applications of graphdiyne-based metal-free catalysts, *Adv. Mater.*, 2019, **31**, 1803762.
29 C. Huang, Y. Li, N. Wang, Y. Xue, Z. Zuo, H. Liu and Y. Li, Progress in research into 2D graphdiyne-based materials, *Chem. Rev.*, 2018, **118**, 7744–7803.
30 X. Gao, H. Liu, D. Wang and J. Zhang, Graphdiyne: synthesis, properties, and applications, *Chem. Soc. Rev.*, 2019, **48**, 908–936.
31 N. Wang, J. He, K. Wang, Y. Zhao, T. Jiu, C. Huang and Y. Li, Graphdiyne-based materials: preparation and application for electrochemical energy storage, *Adv. Mater.*, 2019, **31**, 1803202.
32 R. Sakamoto, N. Fukui, H. Maeda, R. Matsuoka, R. Toyoda and H. Nishihara, The accelerating world of graphdiynes, *Adv. Mater.*, 2019, **31**, 1804211.
33 Y. Du, W. Zhou, J. Gao, X. Pan and Y. Li, Fundament and application of graphdiyne in electrochemical energy, *Acc. Chem. Res.*, 2020, **53**, 459–469.
34 Z. Zuo and Y. Li, Emerging electrochemical energy applications of graphdiyne, *Joule*, 2019, **3**, 899–903.
35 J. Guo, M. Guo, F. Wang, W. Jin, C. Chen, H. Liu and Y. Li, Graphdiyne: Structure of Fluorescent Quantum Dots, *Angew. Chem., Int. Ed.*, 2020, **59**, 16712–16716.
36 Z. Zuo, F. He, F. Wang, L. Li and Y. Li, Spontaneously splitting copper nanowires into quantum dots on graphdiyne for suppressing lithium dendrites, *Adv. Mater.*, 2020, **32**, 2004379.
37 H. Yu, Y. Xue and Y. Li, Graphdiyne and its assembly architectures: synthesis, functionalization, and applications, *Adv. Mater.*, 2019, **31**, 1803101.
38 Y. Xue, B. Huang, Y. Yi, Y. Guo, Z. Zuo, Y. Li, Z. Jia, H. Liu and Y. Li, Anchoring zero valence single atoms of nickel and iron on graphdiyne for hydrogen evolution, *Nat. Commun.*, 2018, **9**, 1460.
39 L. Hui, Y. Xue, B. Huang, H. Yu, C. Zhang, D. Zhang, D. Jia, Y. Zhao, Y. Li, H. Liu and Y. Li, Overall water splitting by graphdiyne-exfoliated and -sandwiched layered double-hydroxide nanosheet arrays, *Nat. Commun.*, 2018, **9**, 5309.
40 H. Yu, Y. Xue, L. Hui, C. Zhang, Y. Li, Z. Zuo, Y. Zhao, Z. Li and Y. Li, Efficient hydrogen production on a 3D flexible heterojunction material, *Adv. Mater.*, 2018, **30**, 1707082.
41 H. Liu, Z. Zhang, C. Wu, Q. Pan, Y. Zhao and Z. Li, Interfacial synthesis of conjugated crystalline 2D fluorescent polymer film containing aggregation-induced emission unit, *Small*, 2019, **15**, 1804519.
42 Q. Pan, S. Chen, C. Wu, Z. Zhang, Z. Li and Y. Zhao, Sulfur-rich graphdiyne-containing electrochemical active tetrathiafulvalene for highly efficient lithium atorage application, *ACS Appl. Mater. Interfaces*, 2019, **11**, 46070–46076.
43 Q. Pan, S. Chen, C. Wu, F. Shao, J. Sun, L. Sun, Z. Zhang, Y. Man, Z. Li, L. He and Y. Zhao, Direct synthesis of crystalline graphtetrayne—a new graphyne allotrope, *CCS Chem.*, 2020, **2**, 1368–1375.
44 Y. Zhao, J. Wan, H. Yao, L. Zhang, K. Lin, L. Wang, N. Yang, D. Liu, L. Song, J. Zhu, L. Gu, L. Liu, H. Zhao, Y. Li and D. Wang, Few-layer graphdiyne doped with sp-hybridized nitrogen atoms at acetylenic sites for oxygen reduction electrocatalysis, *Nat. Chem.*, 2018, **10**, 924–931.
45 S. Zhang, Y. Cai, H. He, Y. Zhang, R. Liu, H. Cao, M. Wang, J. Liu, G. Zhang, Y. Li, H. Liu and B. Li, Heteroatom doped graphdiyne as efficient metal-free electrocatalyst for oxygen reduction reaction in alkaline medium, *J. Mater. Chem. A*, 2016, **4**, 4738–4744.
46 H. Shang, Z. Zuo, H. Zheng, K. Li, Z. Tu, Y. Yi, H. Liu, Y. Li and Y. Li, N-doped graphdiyne for high-performance electrochemical electrodes, *Nano Energy*, 2018, **44**, 144–154.
47 C. Xing, Y. Xue, B. Huang, H. Yu, L. Hui, Y. Fang, Y. Liu, Y. Zhao, Z. Li and Y. Li, Fluorographdiyne: a metal-free catalyst for applications in water reduction and oxidation, *Angew. Chem., Int. Ed.*, 2019, **58**, 13897–13903.
48 T. Tanaka and A. Osuka, Conjugated porphyrin arrays: synthesis, properties and applications for functional materials, *Chem. Soc. Rev.*, 2015, **44**, 943–969.
49 S. Shaik, H. Hirao and D. Kumar, Reactivity of high-valent Iron–Oxo species in enzymes and synthetic eeagents: a tale of many states, *Acc. Chem. Res.*, 2007, **40**, 532–542.
50 Z. Gross, The groves–psiro dioxomanganese(V) story, *Angew. Chem., Int. Ed.*, 2008, **47**, 2737–2739.
51 Y. Zhu, B. Zhang, X. Liu, D. W. Wang and D. S. Su, Unravelling the structure of electrocatalytically active Fe–N complexes in carbon for the oxygen reduction reaction, *Angew. Chem., Int. Ed.*, 2014, **53**, 10673–10677.
52 S.-i. Yamazaki, Metalloporphyrins and related metallomacrocycles as electrocatalysts for use in polymer electrolyte fuel cells and water electrolyzers, *Coord. Chem. Rev.*, 2018, **373**, 148–166.
53 H. Huang, F. Li, Y. Zhang and Y. Chen, Two-dimensional graphdiyne analogues porphyrin covalent organic framework nanosheets as stable electrocatalyst for oxygen evolution reaction, *J. Mater. Chem. A*, 2019, **7**, 5575–5582.
54 A. Wang, L. Cheng, W. Zhao, X. Shen and W. Zhu, Electrochemical hydrogen and oxygen evolution reactions from a cobalt-porphyrin-based covalent organic polymer, *J. Colloid Interface Sci.*, 2020, **579**, 598–606.
55 A. Wang, W. Zhao, X. Chen, Y. Yang, W. Zhu and D. Shang, Coordination-induced broadband optical nonlinearity through axial bonding of pyridine anchored methine-bridged polypyrrole to metal-porphyrins, *Dyes Pigm.*, 2018, **157**, 20–26.
56 X. Tan, C. Li and M. Li, Synthesis of a two-dimensional porphyrin framework connected by 1,3-diyne linkages via in situ deprotection of trimethylsilicon at a water/oil interface, *Polym. Int.*, 2021, **70**, 277–281.
57 J. Li, X. Gao, X. Jiang, X.-B. Li, Z. Liu, J. Zhang, C.-H. Tung and L.-Z. Wu, Graphdiyne: a promising catalyst–support to stabilize cobalt nanoparticles for oxygen evolution, *ACS Catal.*, 2017, **7**, 5209–5213.

58 J. He, S. Y. Ma, P. Zhou, C. X. Zhang, C. He and L. Z. Sun, Magnetic properties of single transition-metal atom absorbed graphdiyne and graphyne sheet from DFT+U calculations, *J. Phys. Chem. C*, 2012, **116**, 26313–26321.
59 X. Cui, H. Li, Y. Wang, Y. Hu, L. Hua, H. Li, X. Han, Q. Liu, F. Yang, L. He, X. Chen, Q. Li, J. Xiao, D. Deng and X. Bao, Room-temperature methane conversion by graphene-confined single iron atoms, *Chem*, 2018, **4**, 1902–1910.
60 A. Covacci, J. L. Telford, G. D. Giudice, J. Parsonnet and R. Rappuoli, Helicobacter pylori virulence and genetic geography, *Science*, 1999, **284**, 1328–1333.